

Computationally efficient methods for modelling laser wakefield acceleration in the blowout regime

B. M. COWAN¹†, S. Y. KALMYKOV²‡, A. BECK³
 X. DAVOINE⁴, K. BUNKERS², A. F. LIFSCHITZ⁵,
 E. LEFEBVRE⁴, D. L. BRUHWILER¹,
 B. A. SHADWICK², AND D. P. UMSTADTER²

¹Tech-X Corporation, 5621 Arapahoe Ave. Ste. A, Boulder, CO 80303, USA

²Department of Physics and Astronomy, University of Nebraska – Lincoln, NE 68588-0299, USA

³Centrum voor Plasma-Astrofysica, Departement Wiskunde, Katholieke Universiteit Leuven, Celestijnenlaan 200B, B-3001 Leuven, Belgium

⁴CEA, DAM, DIF, Arpajon F-91297, France

⁵Laboratoire d'Optique Appliquée, ENSTA, Ecole Polytechnique, CNRS, 91761 Palaiseau, France

(Received ?; revised ?; accepted ?. - To be entered by editorial office)

Electron self-injection and acceleration until dephasing in the blowout regime is studied for a set of initial conditions typical of recent experiments with 100 terawatt-class lasers. Two different approaches to computationally efficient, fully explicit, three-dimensional particle-in-cell modelling are examined. First, the Cartesian code VORPAL (Nieter & Cary 2004) using a perfect-dispersion electromagnetic solver precisely describes the laser pulse and bubble dynamics, taking advantage of coarser resolution in the propagation direction, with a proportionally larger time step. Using third-order splines for macroparticles helps suppress the sampling noise while keeping the usage of computational resources modest. The second way to reduce the simulation load is using reduced-geometry codes. In our case, the quasi-cylindrical code CALDER-CIRC (Lifschitz *et al.* 2009) uses decomposition of fields and currents into a set of poloidal modes, while the macroparticles move in the Cartesian 3D space. Cylindrical symmetry of the interaction allow using just two modes, reducing the computational load to roughly that of a planar Cartesian simulation while preserving the 3D nature of the interaction. This significant economy of resources allows using fine resolution in the direction of propagation and a small time step, making numerical dispersion vanishingly small, together with a large number of particles per cell, enabling good particle statistics. Quantitative agreement of the two simulations indicates that they are free of numerical artefacts. Both approaches thus retrieve physically correct evolution of the plasma bubble, recovering the intrinsic connection of electron self-injection to the nonlinear optical evolution of the driver.

1. Introduction

Relativistic Langmuir waves driven by short, intense laser pulses in rarefied plasmas maintain accelerating gradients several orders of magnitude higher than those accessible in conventional metallic structures (Tajima & Dawson 1979; Gorbunov & Kirsanov 1987;

† Email address for correspondence: benc@txcorp.com

‡ Email address for correspondence: skalmykov2@unl.edu

Esarey *et al.* 2009). The technical simplicity and compactness of these laser-plasma accelerators (LPAs) is attractive for a broad range of applications, such as nuclear activation and on-site isotope production (Leemans *et al.* 2001; Reed *et al.* 2007), long-distance probing of defects in shielded structures (Ramanathan *et al.* 2010), and testing radiation resistivity of electronic components (Hidding *et al.* 2011). Realisation of compact, inexpensive, bright x- and gamma-ray sources using electron beams from LPAs (Rousse *et al.* 2004, 2007; Ta Phuoc *et al.* 2005; Kneip *et al.* 2010; Cipiccia *et al.* 2011) holds the promise to enable a much wider user community than can be served by existing large-scale facilities. These applications are not especially demanding as regards electron beam quality, and in fact sometimes draw benefits from poor beam collimation and a broad energy spectrum (Hidding *et al.* 2011). However, there are also important applications with much tighter beam requirements. Such applications include generating coherent x-rays using an external magnetic undulator (Grüner *et al.* 2007; Schlenvoigt *et al.* 2008*b,a*; Fuchs *et al.* 2009), producing x-rays for the phase contrast imaging (Fourmaux *et al.* 2011; Kneip *et al.* 2011), and high-brightness, quasi-monochromatic gamma-ray Compton sources (Leemans *et al.* 2005; Hartemann *et al.* 2007); these require electron beams with a multi-kA current, low phase space volume, and energy in the few-gigaelectronvolt (GeV) range.

Achieving this high level of accelerator performance is a major near-term goal of the LPA community. Modern laser systems capable of concentrating up to 10 Joules of energy in a sub-50 femtosecond pulse (Yanovsky *et al.* 2008; Froula *et al.* 2009; Kneip *et al.* 2009; Fourmaux *et al.* 2011) make it possible to achieve the so-called blowout (or “bubble”) regime, which is desirable due to its technical simplicity and scalability (Gordienko & Pukhov 2005; Lu *et al.* 2007). In this regime, motion of the electrons in the focus of the laser pulse is highly relativistic. The laser ponderomotive force expels plasma electrons from the region of the pulse, while the fully stripped ions remain essentially immobile, creating a column of positive charge in the laser wake. The charge separation force attracts bulk plasma electrons to the axis, creating a closed bubble devoid of electrons. This co-propagating electron density bubble (Rosenzweig *et al.* 1991; Mora & Antonsen 1996; Pukhov & Meyer-ter-Vehn 2002; Gordienko & Pukhov 2005; Lu *et al.* 2006) guides the laser pulse over many Rayleigh lengths (Mora & Antonsen 1996; Lu *et al.* 2007). The bubble readily traps initially quiescent background electrons, accelerating them to hundreds of megaelectronvolts (MeV) over a few mm, creating a collimated electron bunch (Pukhov & Meyer-ter-Vehn 2002; Kalmykov *et al.* 2011*a*). It is in this regime that the first quasi-monoenergetic electrons were produced from laser plasmas in the laboratory (Geddes *et al.* 2004; Mangles *et al.* 2004; Faure *et al.* 2004), and the GeV energy range was approached (Leemans *et al.* 2006; Karsch *et al.* 2007; Hafz *et al.* 2008; Froula *et al.* 2009; Kneip *et al.* 2009; Clayton *et al.* 2010; Lu *et al.* 2011; Liu *et al.* 2011; Pollock *et al.* 2011).

Multi-dimensional particle-in-cell (PIC) simulations have played a key role in understanding the physics of the fully kinetic, strongly relativistic blowout regime. The PIC method (Hockney & Eastwood 1981; Birdsall & Langdon 1985) self-consistently models both electromagnetic fields and charged particles, representing field quantities on a grid and particles in a continuous phase space. Given sufficient computing power, electromagnetic PIC codes can simulate the plasma electrons (and ions, if necessary), the laser pulse driving the plasma wake, and the dynamics of electrons injected into the accelerating potential. In particular, two- and three-dimensional PIC simulations have been essential in understanding the dynamical nature of the electron self-injection process (Xu *et al.* 2005; Oguchi *et al.* 2008; Wu *et al.* 2009; Zhidkov *et al.* 2010; Kalmykov *et al.* 2009, 2010, 2011*a,b,c*). However, to capture precisely the correlation between driver dynamics, elec-

tron self-injection, and GeV-scale acceleration in the bubble regime, a simulation must meet a number of challenging requirements.

Optimisation of a GeV-scale LPA performance, even with the use of massively parallel computation, is a challenging task especially because of the necessary cm-scale laser-plasma interaction length. The laser energy is used most effectively if electrons are accelerated until they outrun the bubble and exit the accelerating phase, at which point they will have gained the maximum possible energy in an LPA stage,

$$E_d \approx 2.7\gamma_g^{4/3} P_{\text{TW}}^{1/3} \text{ MeV}. \quad (1.1)$$

Acceleration to this *dephasing limit* occurs over the distance (Lu *et al.* 2007)

$$L_d \approx 0.6\lambda_0\gamma_g^{8/3} P_{\text{TW}}^{1/6}. \quad (1.2)$$

Here, P_{TW} is the laser power in terawatts ($1 \text{ TW} = 10^{12} \text{ W}$), $\gamma_g = \omega_0/\omega_{\text{pe}} \gg 1$ is the Lorentz factor associated with the linear group velocity of the pulse in plasma, ω_0 is the laser frequency, $\lambda_0 = 2\pi c/\omega_0$ is the laser wavelength, $\omega_{\text{pe}} = (n_0 e^2/m_e \epsilon_0)^{1/2}$ is the electron Langmuir frequency, m_e is the electron rest mass, n_0 is the background electron density, e is the electron charge, and ϵ_0 is the permittivity of free space. The scalings (1.1) and (1.2) imply that the pulse remains self-guided, namely, that it remains longer than $c\omega_{\text{pe}}^{-1}$ (Sprangle *et al.* 1990; Gorbunov *et al.* 2005), and that its power exceeds the critical power for relativistic self-focusing, $P_{\text{cr}} = 16.2\gamma_g^2 \text{ GW}$ (Sun *et al.* 1987). Increasing the electron energy therefore requires reduction of the electron plasma density, increasing both the bubble velocity and size,

$$L_{\text{acc}} \approx 0.9\lambda_0\gamma_g^{2/3} P_{\text{TW}}^{1/6}, \quad (1.3)$$

where L_{acc} is the length of the accelerating phase of the wakefield (roughly equal to the bubble radius). Electron dephasing scales as $L_d \sim n_0^{-4/3}$ and thus the final energy gain scales as $E_d \sim n_0^{-2/3}$. For instance, reaching 1 GeV energy with a 200 TW pulse and a wavelength of $\lambda_0 = 0.8 \mu\text{m}$ may be achieved in a 0.47 cm length plasma with density $n_0 = 3.5 \times 10^{18} \text{ cm}^{-3}$, and doubling that energy would require nearly four times the plasma length and three times lower density, also increasing the bubble size by $\sim 40\%$. Simulations of LPA commonly use a moving-widow, where the simulation box propagates with the speed of light colinearly with the laser pulse. This optimisation notwithstanding, even the experiments with currently operating 100 TW systems bring forth the task of modelling the pulse propagation in cm-length plasmas, with the size of 3D simulation box on the order of hundred(s) of microns longitudinally and transversely.

The greatest challenge arises from the great disparity of physical scales between the laser wavelength and plasma length, which is the hallmark of high-energy laser-plasma acceleration. The need to resolve the laser wavelength, $\lambda_0 \sim 1 \mu\text{m}$, fixes the grid resolution, and, due to stability conditions (Courant *et al.* 1967), also limits the time step to a small fraction of ω_0^{-1} . Furthermore, the strong localisation of the injection process imposes even stricter limit on grid resolution; the vast majority of injection candidates are concentrated in the inner lining of the bubble (the sheath), and penetrate into the bubble near its rear, where the sheath is longitudinally compressed to a few tens of nanometres (Wu *et al.* 2009; Kalmykov *et al.* 2011a). Resolving this structure, together with ensuring sufficient particle statistics in the sheath, is necessary to avoid excessive sampling noise and eliminate unphysical effects. In this situation, extending the plasma length to centimeters and increasing the size of the simulation window to hundreds of microns, while at the same time maintaining sufficient macroparticle statistics, would require solving Maxwell's equations on meshes amounting to billions of grid points, and advancing 1–

10 billion macroparticles over millions of time steps. Performing such simulations with standard electromagnetic solvers and particle movers requires a national-scale supercomputing facility. As a result, an attempt to reproduce the long time scale evolution of the laser and the bubble together with fine details of the electron self-injection dynamics is usually a compromise between affordable simulation load and unavoidable coarseness of the results. However, the high precision of modern LPA experiments and high beam quality requirements of the applications are rather unforgiving to these compromises and do not tolerate numerical artefacts (Cormier-Michel *et al.* 2008).

These considerations make it clear that PIC algorithms must be modified in order to reduce the required computational resources without compromising precision. One of the main directions is development of electromagnetic solvers that minimize numerical error while using the lowest possible grid resolution. One particular limitation of PIC that requires high longitudinal resolution is that of numerical dispersion. In PIC, electromagnetic fields are typically updated using the finite-difference time-domain (FDTD) method on a staggered Yee grid (Yee 1966; Taflov & Hagness 2005). This method is second-order accurate, and since it is explicit and local, it parallelizes efficiently enabling large-scale simulations. However, it is known that this algorithm experiences numerical dispersion error for waves propagating along the axis, which leads to errors in the group velocity of the laser pulse. This artificial slowdown of the driver and the bubble leads to incorrect dephasing of accelerated electrons and also permits synchronisation of the sheath electrons with the bubble, leading to their unphysical injection. Mitigating this effect by using higher resolution increases the computation time quadratically. Because of the deleterious effects of numerical dispersion in FDTD schemes, efforts have been made to develop *perfect dispersion* algorithms, which exhibit no numerical dispersion for waves propagating along a grid axis. For accelerator applications, several modifications to FDTD have been described that correct for numerical dispersion using implicit methods (Zagorodnov *et al.* 2003; Zagorodnov & Weiland 2005). Because LPA simulations tend to be quite large-scale (using thousands of processor cores), an explicit algorithm is desirable for reasons of computational efficiency. Such an algorithm has been described in 2D (Pukhov 1999) and in 3D for cubic cells (Kärkkäinen *et al.* 2006). These algorithms have also been explored for LPA as a means of reducing noise in boosted-frame simulations (Vay *et al.* 2011).

In this paper, we use two complementary simulation codes (with different numerical approaches and physics content) to explore physical phenomena involved in self-injection and acceleration of electrons until dephasing under typical conditions of recent experiments with 100 TW-class lasers. We use a newly-developed perfect-dispersion algorithm (Cowan *et al.* 2012) implemented in the fully explicit 3D Cartesian VORPAL simulation framework (Nieter & Cary 2004), subsequently referred to as VORPAL-PD. The algorithm, briefly described in Sec. 2, eliminates numerical dispersion in the direction of pulse propagation. Thus, even with a relatively large longitudinal grid spacing (~ 15 grid points per λ_0), the correct group velocity of a broad-bandwidth laser pulse is obtained.

The other code used here, CALDER-CIRC, uses cylindrical geometry. This code uses poloidal mode decomposition of fields and currents defined on a radial grid, while macroparticles retain their full 3D dynamics in Cartesian coordinates (Lifschitz *et al.* 2009). Well-preserved cylindrical symmetry of the laser-plasma interaction enables using just a few lower-order modes. Neglecting higher-order, non-axisymmetric contributions to the wakefields and currents makes it possible to approach the performance of a 2D code. CALDER-CIRC thus allows for fast, extra-high resolution runs with excellent macroparticle statistics (Kalmykov *et al.* 2010, 2011a).

The paper is organized as follows. In section 2 we outline the main features of the

recently implemented perfect dispersion algorithm in the VORPAL-PD code. Section 3 is dedicated to the benchmarking of VORPAL-PD against CALDER-CIRC. Sec. 4 summarizes the results and indicates the directions of future work.

2. The perfect dispersion method

In this section we give a brief overview of the perfect dispersion method we use; a more complete description together with detailed benchmarks will be presented in (Cowan *et al.* 2012). Our method is based on that in (Pukhov 1999; Kärkkäinen *et al.* 2006), in which the FDTD algorithm is modified by smoothing the fields in the curl operator in one of Maxwell's equations. We choose to smooth the electric fields for the magnetic field update; our update equations are then

$$D_t \mathbf{B} = -\nabla' \times \mathbf{E}, \quad D_t \mathbf{E} = c^2 \nabla \times \mathbf{B} - \frac{\mathbf{J}}{\epsilon_0}, \quad (2.1)$$

where \mathbf{J} is the electric current deposited from particle motion. Here D_t is the finite difference time derivative, $\nabla \times$ is the standard finite difference curl operator, and $\nabla' \times$ is the modified curl operator. Our modification to the curl operator involves applying smoothing transverse to the coordinate axis along which the derivative is taken. For instance, when computing $\partial E_y / \partial x$, E_y is smoothed in the y and z directions. This is equivalent to applying a smoothing operator before the numerical derivative operator. The electric field is smoothed only for the update of the magnetic field; the smoothed fields are not stored for the next time step.

The smoothed curl operator $\nabla' \times$ is formed by modifying the finite difference operation. If D_i is the numerical derivative operator in the i -th direction, then for the modified curl we use $D_i S_i$ in place of D_i , where S_i is the smoothing operator for the derivative. The smoothing operator S_x is defined by the stencil in the y and z directions

$$\begin{bmatrix} \gamma_{yz} & \beta_z & \gamma_{yz} \\ \beta_y & \alpha_x & \beta_y \\ \gamma_{yz} & \beta_z & \gamma_{yz} \end{bmatrix}, \quad (2.2)$$

and similar relations hold for cyclic permutations of the coordinate indices. The coefficients α_i , β_i , and γ_{ij} are chosen to guarantee that waves propagating along the x axis (the laser propagation direction in our simulations) in vacuum experience no numerical dispersion, as described in (Cowan *et al.* 2012). The only constraint is that the longitudinal grid spacing Δx must satisfy $\Delta x \leq \Delta y, \Delta z$ for the transverse grid spacings Δy and Δz .

3. Benchmarking

While a technological path to high-quality GeV beams exists, experimental progress is impeded by an incomplete understanding of the intrinsic relation between electron self-injection and nonlinear optical evolution of the driver, and hence by the lack of suitable criteria for selection of the optimal regimes that produce beams with the smallest possible phase-space volume. Control and optimisation of the fully kinetic, intrinsically 3D process of electron self-injection is a daunting task. It involves a systematic study of the links among the dynamics of self-injection and the nonlinear optical processes involving the laser pulse and the bubble.

Due to the extended acceleration length, the interaction of the laser pulse with the plasma is rich in nonlinear phenomena. Even a Gaussian beam which is perfectly matched

to the electron density gradient in which it propagates is not immune to nonlinear optical processes. Oscillations of the pulse spot-size due to non-linear refraction (Oguchi *et al.* 2008; Zhidkov *et al.* 2010; Kalmykov *et al.* 2010), self-phase modulation leading to the formation of a relativistically intense optical piston (Tsung *et al.* 2002; Lontano & Murusidze 2003; Faure *et al.* 2005; Pai *et al.* 2010; Vieira *et al.* 2010; Kalmykov *et al.* 2011*a,b*), and relativistic filamentation (Andreev *et al.* 2007; Thomas *et al.* 2007, 2009) are processes which result in pulse deformations. Electron self-injection appears to be extremely sensitive to such changes in pulse shape, which lead to contamination of the electron beam with polychromatic, poorly collimated background (Kalmykov *et al.* 2011*b*). Such contamination is readily seen even in simulations with idealised initial conditions (Kneip *et al.* 2009; Froula *et al.* 2009; Martins *et al.* 2010; Kalmykov *et al.* 2010, 2011*a*). The complicated modal structure of the incident pulse further aggravates the situation, leading to continuous off-axis injection, collective betatron oscillations (Glinec *et al.* 2008; Mangles *et al.* 2009; Cummings & Thomas 2011), and electron beam steering (Popp *et al.* 2010). In practice, these phenomena currently preclude operation reliable enough to enable high-precision user experiments; reported islands of stability for self-injection in laser and plasma parameter space remain relatively narrow (Karsch *et al.* 2007; Mangles *et al.* 2007; Thomas *et al.* 2007; Hafz *et al.* 2008; Maksimchuk *et al.* 2008; Wiggins *et al.* 2010). Numerical codes used in predictive modelling of LPAs must be able to reproduce these phenomena with high precision in order not to confuse the instability of acceleration caused by physical processes with unphysical artefacts caused by intrinsic deficiencies of numerical algorithms, such as numerical dispersion, high sampling noise, and grid heating.

3.1. Simulation parameters

The simulations presented here extend the earlier case study by (Kalmykov *et al.* 2011*a*) and use the same set of initial conditions. A transform-limited Gaussian laser pulse with full width at half-maximum (FWHM) in intensity $\tau_L = 30$ fs, wavelength $\lambda_0 = 0.805$ μm , and 70 TW power is focussed at the plasma border ($x = 0$) into a spot size $r_0 = 13.6$ μm , and propagates in the positive x direction. The laser pulse is polarised in the y direction. The peak intensity at the focus is 2.3×10^{19} W/cm², giving a normalised vector potential of $a_0 = 3.27$. The plasma density has a 0.5 mm linear entrance ramp followed by a 2 mm plateau and a 0.5 mm linear exit ramp. The density in the plateau region, $n_0 = 6.5 \times 10^{18}$ cm⁻³, corresponds to $\gamma_g \approx P/P_{\text{cr}} \approx 16.3$ and dephasing length $L_d \approx 1.7$ mm.

The simulations carried out with VORPAL-PD use grid spacings of $\Delta x = 0.06\lambda_0 = 48.3$ nm longitudinally and $\Delta y = \Delta z = 0.5\lambda = 403$ nm transversely, with four macroparticles per cell. Use of third-order splines for the macroparticle shapes reduces the sampling noise, mitigating the adverse effect of the coarse grid. The domain in the VORPAL-PD simulation is 72 μm long and 91 μm wide, and is surrounded transversely by a 16-layer perfectly-matched layer absorbing boundary. The code is fully parallelised, and was run using 6144 cores on the Hopper supercomputer at the National Energy Research Scientific Computing Center (NERSC). Completion of a typical run took $\sim 3 \times 10^5$ CPU hours.

The CALDER-CIRC simulation uses 45 macroparticles per cylindrical cell, formed by the revolution of the grid cell around the propagation axis. The longitudinal grid spacing is $\Delta x = 0.125c/\omega_0 \approx 16$ nm. The aspect ratio $\Delta r/\Delta x = 15.6$ (where $r = \sqrt{y^2 + z^2}$), and the time step $\Delta t = 0.1244\omega_0^{-1}$. With these grid parameters, numerical dispersion is negligible, and sampling noise is significantly reduced. This high resolution simulation does not indicate any new physical effects compared to the VORPAL-PD simulation, and does not exhibit significant differences in the quantitative results. Well preserved

cylindrical symmetry during the interaction (confirmed in the VORPAL-PD simulation) enables us to approximate fields and currents using just the two lowest-order poloidal modes, thus reducing the 3D problem to an essentially 2D one. These results confirm the earlier established fact (Lifschitz *et al.* 2009) that, in the case of a linearly polarised laser, higher-order modes contribute only weakly to the electric field. Comparison with the results of the VORPAL-PD runs shows that our restriction to only two modes is sufficiently precise to reproduce all relevant physical effects, and to simulate the propagation through a 3 mm plasma in 2 625 CPU hours on 250 cores.

3.2. Formation of quasi-monoenergetic bunches and physical origin of dark current

Upon entering the plasma, the strongly overcritical pulse rapidly self-focuses, reaching its highest intensity at $x \approx 0.8$ mm, soon after entering the density plateau. Full blowout is maintained over the entire propagation distance. In both simulations, electrons are accelerated until dephasing in two distinct stages, each characterised by completely different laser pulse dynamics. *Transverse* evolution of the laser pulse is the hallmark of Stage I. The pulse spot size oscillates, first causing expansion and then contraction of the bubble. The bubble expansion produces self-injection of electrons from the sheath; stabilisation and contraction of the bubble extinguish injection, limiting the beam charge to a fraction of a nC. Phase space rotation creates a well-collimated quasi-monoenergetic bunch long before dephasing. Further acceleration (Stage II) is dominated by *longitudinal (temporal)* self-compression of the pulse, leading to gradual elongation of the bubble and continuous injection, producing a polychromatic, poorly collimated energy tail with a few nC charge. This two-stage evolution has been noticed in earlier simulations (Froula *et al.* 2009; Kneip *et al.* 2009), and explained in detail in (Kalmykov *et al.* 2011a).

The correlation between the plasma bubble evolution and the self-injection process is quantified in figure 1. Panel (a) shows the length of the accelerating phase on axis, viz. the length of the region inside the bubble where the longitudinal electric field is negative. Panel (b) shows the longitudinal “collection phase space”, viz. momenta of macroparticles reaching the dephasing point, $p_x(x = x_{\text{deph}})$, vs. their initial position in plasma. Panel (c) shows the collection volume: the initial positions of electrons reaching the dephasing point. Comparison of these three panels shows that *electrons are injected only during the periods of bubble expansion*.

During Stage I, radial oscillation of the laser pulse tail inside the bubble causes alternating expansion and contraction of the first bucket, clearly seen in the progression from $x = 0.6$ to 1.24 mm in figure 1(a). The bubble size oscillates around the average value predicted by the estimate (1.3), $L_{\text{acc}} \approx 9.5 \mu\text{m}$. Electron self-injection into the oscillating bubble leads to the formation of a quasi-monoenergetic component in the energy spectrum. At the end of Stage I, at $z \approx 1.24$ mm, the bubble contracts to the same size in both runs, truncating the tail of injected bunch and expelling electrons injected between $x = 0.825$ and $x \approx 0.95$ mm. These electrons do not reach dephasing and thus are missing in figures 1(b) and 1(c). Electrons injected between $x = 0.65$ and 0.825 mm, remain in the bubble and are further accelerated. This well-separated group of particles is clearly seen in figure 1(b). In both the VORPAL-PD and CALDER-CIRC simulations, these electrons reach dephasing first, preserving low energy spread, and are accelerated to the highest energy, $E \approx 500$ MeV. The bubble expands more rapidly and stabilises sooner in the VORPAL-PD simulation, causing stronger reduction of the phase velocity in the subsequent buckets (second and third). Hence, in contrast to the CALDER-CIRC run, VORPAL-PD gives a noticeable amount of charge trapped and preaccelerated in these buckets. These electrons, indicated by the red ellipse in figure 1(b), are swallowed by the expanding first bucket during Stage II and are further accelerated, contributing to the

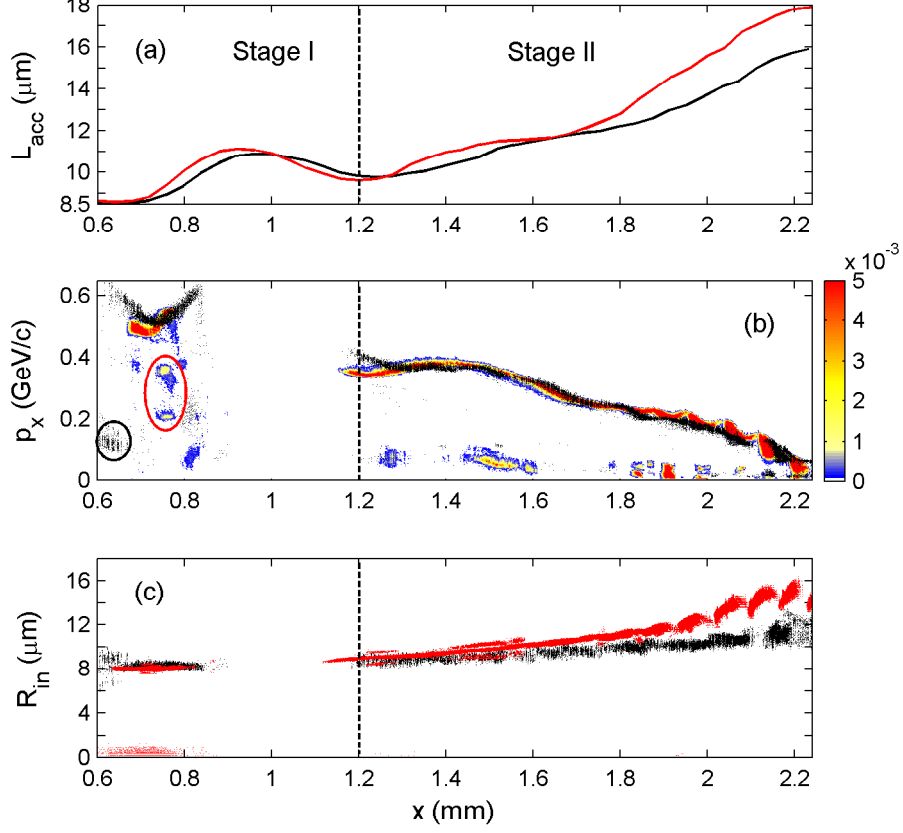


FIGURE 1. (a) Length of the accelerating phase vs. propagation distance in CALDER-CIRC (black) and VORPAL-PD simulations (red/grey). Expansion and contraction of the bubble due to non-linear focusing of the driver (Stage I) is followed by continuous expansion caused by pulse self-compression (Stage II). (b) Longitudinal momentum of electrons reaching the dephasing point, $x_{\text{deph}} \approx 2.4$ mm, vs. their initial longitudinal positions. Black dots are the CALDER-CIRC macroparticles; the colourmap represents the normalised number density of VORPAL-PD macroparticles. Electrons are injected only during periods of bubble expansion. A quasi-monoenergetic bunch forms during Stage I and maintains its low energy spread until dephasing, indicated by the group of early-injected particles with $E \approx 500$ MeV. Groups of electrons encompassed by the ellipses were injected into the second and third buckets, to be further captured and accelerated by the expanding first bucket. Continuous injection during Stage II creates a polychromatic energy tail. (c) Collection volume: initial radial offsets of electrons reaching dephasing limit $R_{\text{in}} = \sqrt{y_{\text{in}}^2 + z_{\text{in}}^2}$, vs. their initial longitudinal positions x_{in} . Black (red/grey) dots are CALDER-CIRC (VORPAL-PD) macroparticles. This collection volume indicates that the vast majority of electrons are collected from a hollow conical cylinder with a radius slightly smaller than the local bubble size.

dark current. This contribution, however, appears to be fairly minimal in comparison to the amount of continuously injected charge during Stage II.

The leading edge of the laser pulse constantly experiences a negative gradient of the nonlinear index of refraction. As a result, by the end of Stage I, it accumulates considerable redshift. During Stage II, plasma-induced group velocity dispersion slows the red-shifted spectral components relative to the unshifted components, leading to the front

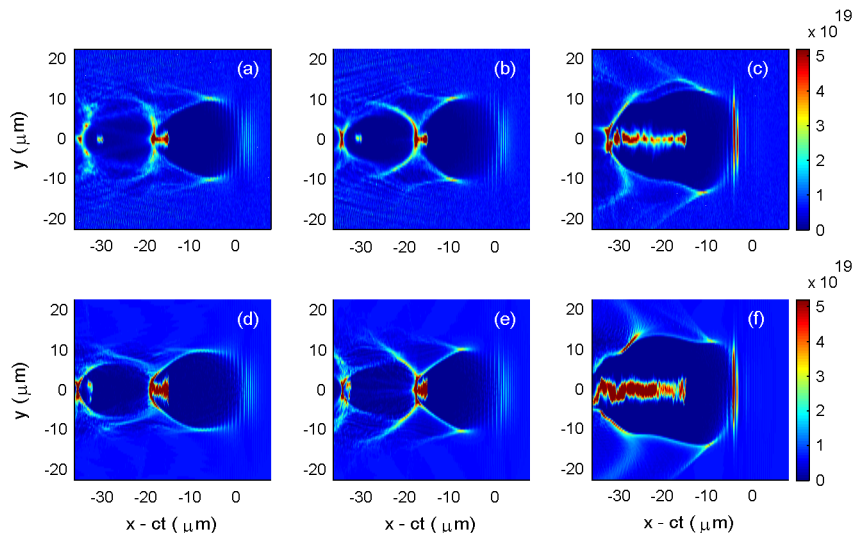


FIGURE 2. Electron density (in cm^{-3}) in the plane of laser polarisation in CALDER-CIRC (top row) and VORPAL-PD simulations (bottom). Panels (a) and (d) show the fully expanded bubble in the middle of Stage I, (b) and (e) the fully contracted bubble at the end of Stage I, and (c) and (f) the bubble in the vicinity of electron dephasing point at the end of Stage II. $x = ct$ is the trajectory of the laser pulse maximum in vacuum; (a) and (d) correspond to the distance $x = ct \approx 930 \mu\text{m}$ from the plasma edge, (b) and (e) to $x = ct \approx 1210 \mu\text{m}$, and (c) and (f) to $x = ct \approx 2364 \mu\text{m}$. Before the dephasing point, the bubble, elongated and deformed due to the laser pulse self-compression, traps considerable charge. Beam loading, however, is yet unable to terminate self-injection (cf. panels (c) and (f)).

etching and pulse self-compressing into a relativistically intense, few-cycle long optical piston (Tsung *et al.* 2002; Lontano & Murusidze 2003; Faure *et al.* 2005; Kalmykov *et al.* 2011a). As the pulse transforms into a piston, the bubble constantly elongates, resulting in copious trapping and creating a poorly collimated, polychromatic tail, clearly seen in figure 1(b). At the dephasing point, $x_{\text{deph}} \approx 2.4 \text{ mm}$, the bubble size becomes nearly twice the estimate $L_{\text{acc}} \approx 9.5 \mu\text{m}$ based on the scaling law (1.3). Even though figure 1(a) shows a larger bubble expansion in the VORPAL-PD run, the sections of collection phase space corresponding to Stage II look nearly identical for both codes in figure 1(b).

The collection volume depicted in figure 1(c) indicates that the electrons are collected from a conical shell with a radius slightly smaller than the bubble radius. This structure of the collection volume indicates that the vast majority of trapped and accelerated electrons have impact parameters of sheath electrons (Tsung *et al.* 2006; Wu *et al.* 2009; Pukhov *et al.* 2010; Kalmykov *et al.* 2010, 2011a). Collection volumes in the VORPAL-PD and CALDER-CIRC runs are almost identical during Stage I, whereas the radius of the cone is larger for VORPAL-PD during Stage II, on account of the greater expansion due to pulse diffraction.

Snapshots of electron density, longitudinal phase space, and energy spectra at the points of maximal expansion and contraction of the bubble are presented in figures 2, 3, and 4. Data for panels (a), (b), and (c) in these figures are from the CALDER-CIRC simulation, and for panels (d), (e), and (f) from the VORPAL-PD simulation.

The fully expanded bubble in the middle of Stage I is shown in figures 2(a) and 2(d). As soon as the bubble fully expands, injection terminates. Uninterrupted injection of sheath electrons before this point produces a large spread of longitudinal momentum and energy, shown in figures 3(a), 3(d), and 4(a).

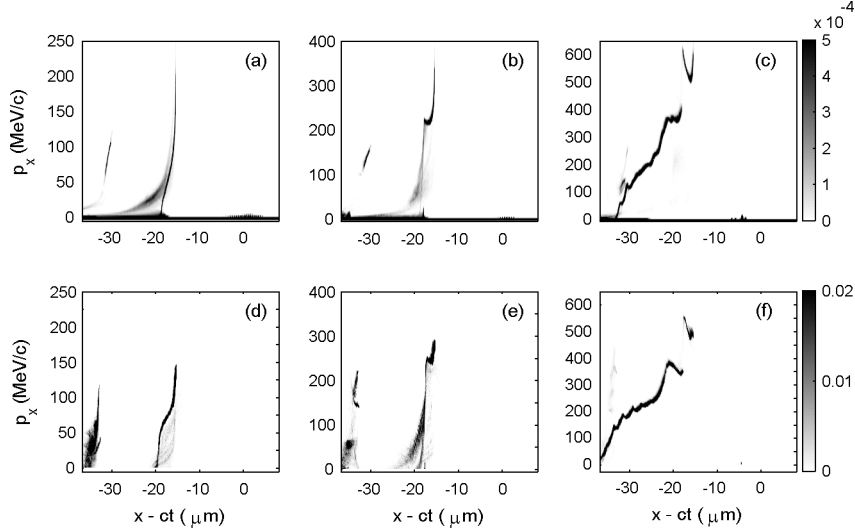


FIGURE 3. Electron density (arbitrary units) in longitudinal phase space in CALDER-CIRC (top row) and VORPAL-PD simulations (bottom). Each panel corresponds to the same panel of figure 2. Full expansion of the bubble saturates injection and initiates phase space rotation (panels (a) and (d)). Contraction of the bubble terminates injection, clipping the rear of injected bunch, eliminating low-energy tail. Phase space rotation makes the bunch quasi-monoenergetic (panels (b) and (e)). Elongation and deformation of the bubble due to the laser pulse self-compression causes continuous injection, producing an electron beam with a continuous spectrum of longitudinal momenta (panels (c) and (f)).

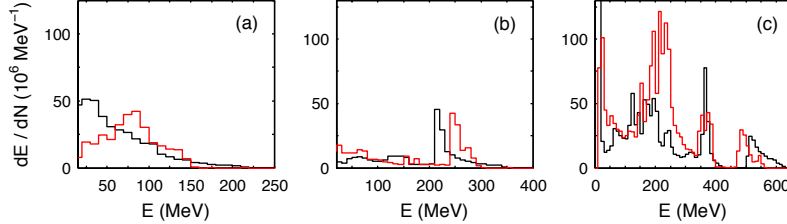


FIGURE 4. Electron energy spectra in CALDER-CIRC (black) and VORPAL-PD simulations (red/grey). Panels (a), (b), and (c) correspond to the phase space snapshots (a) and (d), (b) and (e), and (c) and (f) of figure 3, respectively. (a) At the point of full expansion, the electron energy spectrum is broad. (b) Full contraction of the bubble suppresses the low-energy tail and reduces the energy spread. Electrons from the second bucket contribute to the background, seen in the diffuse peaks around 150 MeV. (c) Continuous injection caused by the bubble expansion and deformation produces a massive polychromatic tail. The leading bunch, at $E \approx 500$ MeV, reaches dephasing, but is still distinct from the tail.

The slight contraction of the bubble between $x = 0.95$ and 1.24 mm truncates the bunch. Electrons injected at the very end of the expansion interval are expelled, while particles remaining in the bucket are further accelerated. The transverse self-fields of the bunch are unable to prevent the bucket contraction. Snapshots of the contracted bubble are presented in figures 2(b) and 2(e). During the contraction interval, the tail of electron bunch, exposed to the highest accelerating gradient, equalises in energy with earlier injected electrons, thus producing a characteristic ‘U’ shape in the longitudinal phase space. This feature (also observed in the similar situation by (Lu *et al.* 2007)) is clearly seen in figures 3(b) and 3(e). As a result of this evolution, quasi-monoenergetic

	Q_{mono}	E_{mono}	ΔE_{mono}	$\varepsilon_{N,y}$	$\varepsilon_{N,z}$
CALDER-CIRC	214	215	20	6.87	7.08
VORPAL-PD	193	245	20	10.7	6.08

TABLE 1. Parameters of the quasi-monoenergetic bunch ($E > 200$ MeV) at the end of Stage I (cf. the spectra in figure 4(b)). Q_{mono} is the charge in pC; E_{mono} is the energy corresponding to the spectral peak (in MeV); ΔE_{mono} is the absolute energy spread (FWHM) in MeV; $\varepsilon_{N,y}$ and $\varepsilon_{N,z}$ are the normalised transverse emittance (in mm mrad) in and out of the laser polarisation plane, respectively.

bunches form in both VORPAL-PD and CALDER-CIRC simulations at the end of Stage I. These quasi-monoenergetic spikes with $< 10\%$ energy spread can be seen in figure 4(b). In addition to the quasi-monoenergetic spikes, these energy spectra also reveal diffuse features near 150 MeV, corresponding to the electrons trapped in the second bucket; these particles can be seen in the snapshots of electron density shown in figures 2(b) and 2(e). These electrons, however, never equalise in energy with the leading high-energy bunch.

Parameters of the bunches, summarised in table 1, appear to be very similar. Normalised transverse emittances presented in this table are calculated according to the usual definition $\varepsilon_{N,i} = (m_e c)^{-1} [(\langle p_i^2 \rangle - \langle p_i \rangle^2)(\langle r_i^2 \rangle - \langle r_i \rangle^2) - (\langle p_i r_i \rangle - \langle r_i \rangle \langle p_i \rangle)^2]^{1/2}$, where $i = y$ and z correspond to the emittance in and out of polarisation plane. The beam asymmetry is more pronounced in the VORPAL-PD simulation, presumably on account of the inclusion of the complete electromagnetic field, in contrast to just two poloidal modes in CALDER-CIRC.

Agreement between the two codes worsens during Stage II. As has already been noted, the bubble expansion is larger in the VORPAL-PD simulation. As a result, the amount of continuously injected charge at the dephasing point (2.5 nC) is about 60% higher and the divergence of the continuously injected beam (80 mrad) is about twice that in the CALDER-CIRC simulation. The difference in charge can be easily inferred from figure 4(c). On the other hand, parameters of the leading bunches are in reasonable agreement, with the central energy 485 ± 20 MeV in VORPAL-PD against 515 ± 25 MeV in CALDER-CIRC run. In both simulations, the emittance of the quasi-monoenergetic component increases by $\sim 30\%$ over its value at the end of Stage I. The lower energy of the leading bunch in the VORPAL-PD run can be explained by its earlier dephasing due to more rapid expansion of the bubble.

Both codes agree that the bubble not only elongates during Stage II, but becomes more and more asymmetric in the laser polarisation plane. The ‘‘pennant-like’’ bubble shape is responsible for massive off-axis injection, leading to the noticeable beam centroid oscillations in the laser polarisation plane seen in figures 2(c) and 2(f). Such phenomenon has been observed in similar situations by others (Glinec *et al.* 2008). This violation of symmetry is a manifestation of carrier-envelope phase effects in the interaction of a relativistically intense, linearly polarised, few-cycle piston with the plasma (Nerush & Kostyukov 2009). Conversely, in the plane orthogonal to the laser polarisation, both the bucket and the beam remain perfectly symmetric (not shown). Surprisingly, the two poloidal radiation modes of CALDER-CIRC still capture the field evolution well. Inclusion of higher order modes should improve the situation. On the other hand, figures 2(c) and 2(f) indicate that electromagnetic solvers of both codes agree on the group velocity of the laser pulse even in the situation where the pulse shrinks down to less than two cycles and remains strongly relativistic. This means that (a) poloidal mode decomposition does not damage dispersion in the axial direction, and (b) the coarse grid and dispersion

properties of VORPAL-PD are sufficient to describe well the extreme case of pulse spectral broadening to $\Delta\omega \sim \omega_0$ and compression to nearly a single cycle.

Examination of the bubble evolution and collection volumes (cf. figure 1), together with individual snapshots of electron density in coordinate and longitudinal phase space, indicate that, in spite of the great difference in the algorithms, VORPAL-PD and CALDER-CIRC reproduce the same correlation between the evolution of the bubble and the self-injection of sheath electrons, and agree quantitatively on the parameters of quasi-monoenergetic beams produced by the oscillating bubble. Self-injection begins, terminates, and resumes at exactly the same positions along the propagation axis in both runs, and electrons are collected from the same plasma volume. Despite differences in minor details, both codes consistently reproduce physical details of the self-injection process over the entire dephasing length. This level of agreement between very different numerical models indicates that the results are largely free of numerical artefacts. Importantly, the discrepancies emerge when the interaction develops noticeable non-cylindrically symmetric features, and hence the reduced field description of CALDER-CIRC loses precision. We believe that the agreement between the models may be improved in a straightforward fashion (viz. using a larger number of poloidal modes) without significantly reducing computational efficiency.

3.3. *Effects of numerical dispersion control*

As described above, simulating upcoming experiments will require economising on computational cost as much as possible without sacrificing physical accuracy. One means of reducing longitudinal resolution requirements, and hence allowing a larger time step, is to minimise numerical dispersion through a modified electromagnetic update. Here we show how numerical dispersion quantitatively affects the injected electron bunch.

The immediate effect of numerical dispersion is an unphysically low group velocity of the laser pulse. While this effect is difficult to observe directly in the laser pulse because of more significant changes in the pulse shape, it can be seen in the electron phase space, which is of experimental importance. We examine the initially-injected electrons at the point where they have rotated in phase space such that the beam has achieved minimal energy spread. The minimal energy spread condition is characterised by the phase space of the bunch being roughly longitudinally symmetric and in the shape of a ‘U’. We find from the perfect dispersion simulation that this occurs after the laser has propagated approximately 1.8 mm into the plasma. We show longitudinal momentum spectra and phase space at this point for both perfect dispersion and normal dispersion in figure 5. We find that with the normal dispersion algorithm, the beam achieves lower energy and exhibits higher energy spread than with the perfect dispersion algorithm. We also find that phase space rotation has occurred more quickly.

We also compare the two dispersion algorithms at points of minimal energy spread. Without dispersion control, the more rapid phase space rotation causes the minimal energy spread to occur after just 1.6 mm of propagation rather than 1.8 mm. We show the two phase space plots in figure 6. This comparison is relevant since for applications, as one would want to design the system such that the injected beam exits the plasma at this point of minimum energy spread (Hafz *et al.* 2011). It is clear from these plots that with the normal dispersion algorithm, the beam has reached lower mean energy (390 MeV) at the minimum energy spread point than with perfect dispersion, where the beam has mean energy of 460 MeV. In addition, the normal dispersion case exhibits slightly higher energy spread and total charge in the bunch.

We also compare the longitudinal momentum spectra and phase space at the points compared with CALDER-CIRC simulations in the previous section, namely 960 μm , 1.24 mm,

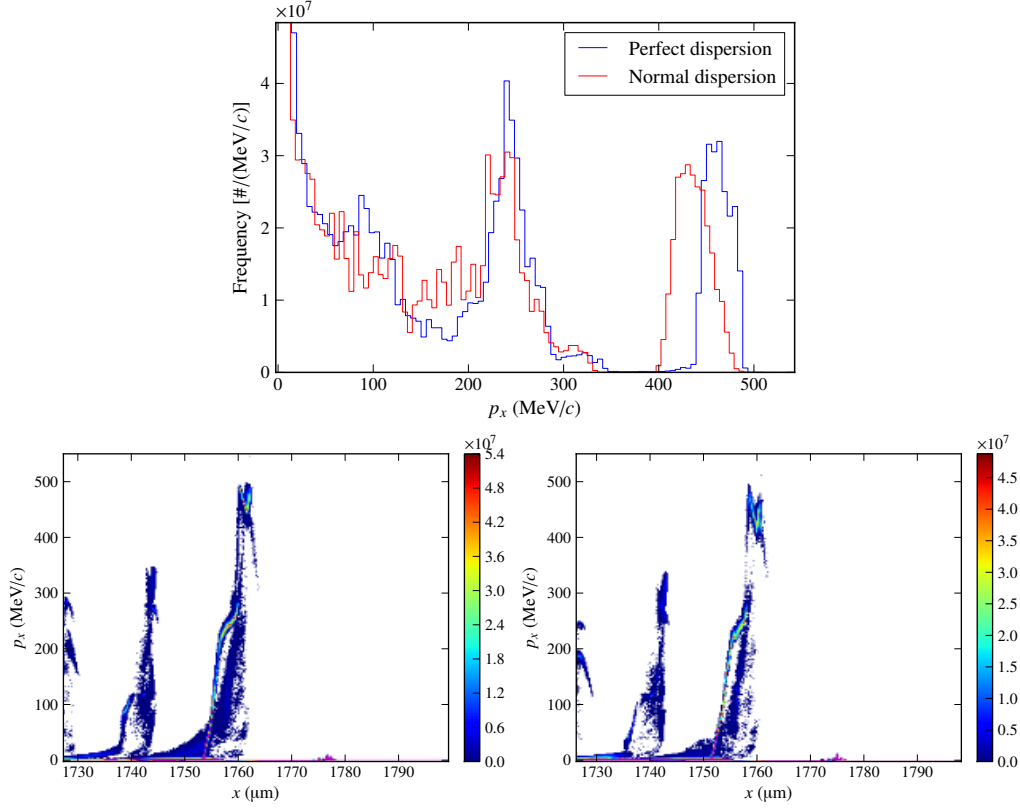


FIGURE 5. Top: Electron longitudinal momentum spectra after 1.8 mm propagation for perfect and normal dispersion. Bottom: Longitudinal phase space for perfect dispersion (left) and normal dispersion (right).

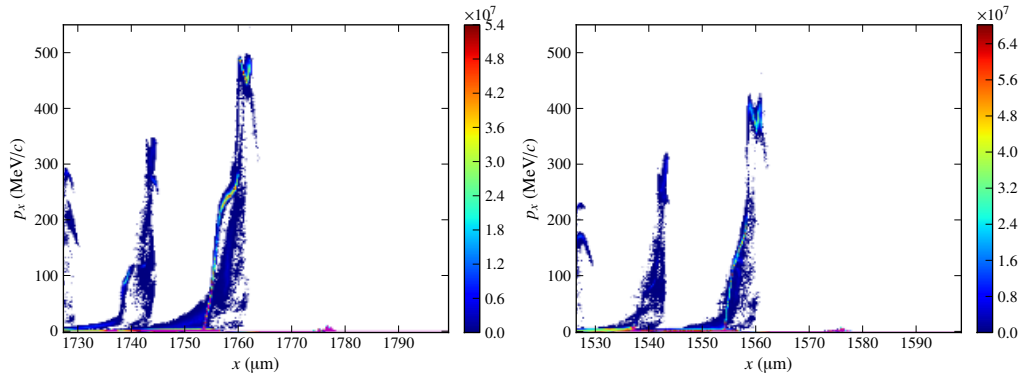


FIGURE 6. Longitudinal phase space for perfect dispersion (left) and normal dispersion (right) at the minimal energy spread point for both algorithms. For perfect dispersion, this is after 1.8 mm of propagation, and for normal dispersion after 1.6 mm.

and 2.4 mm. These comparisons are shown in figure 7. We can see, especially in the later two plots, that the injected bunch in the normal dispersion simulation shows both lower mean energy and greater phase space rotation than in the perfect dispersion run, which agrees better with the CALDER-CIRC simulations as seen in the previous section.

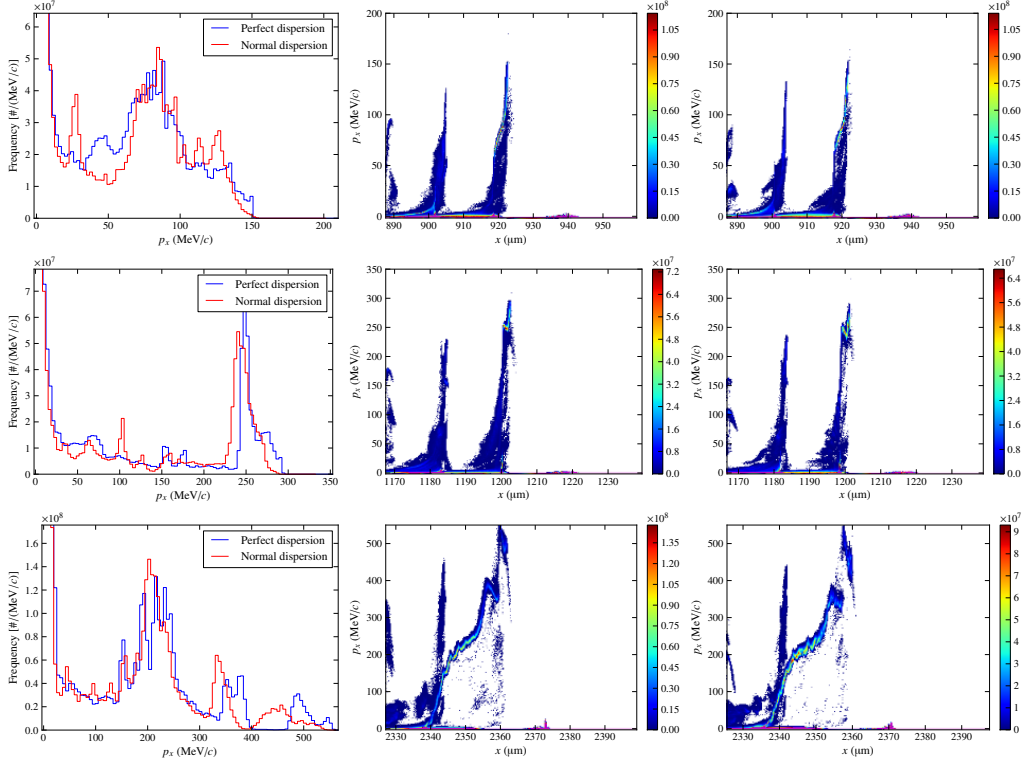


FIGURE 7. Comparisons of longitudinal momentum and phase space. Momentum spectra for perfect and normal dispersion (left), the perfect-dispersion phase space (center), and the normal-dispersion phase space (right). The top row shows the electron distribution at $960\ \mu\text{m}$ of propagation, the middle row at $1.24\ \text{mm}$, and the bottom row at $2.4\ \text{mm}$.

While these discrepancies are small, they are noticeable and consistent with numerical group velocity error. As LPA system designs are refined, and diagnostics and control over the laser pulse and plasma improve, it will be important to control numerical effects on this level to optimise parameters through simulation. The perfect dispersion algorithm allows us to do so while still using low longitudinal resolution for computational efficiency.

4. Conclusions

In this paper we have demonstrated the utility of using computationally efficient, fully explicit 3D PIC codes to describe and explain the physical phenomena accompanying electron acceleration until dephasing in a self-guided LPA in the blowout regime. Electron self-injection and its relation to nonlinear dynamical processes involving the laser pulse and bubble were explored. Two approaches to reducing the computational cost of the simulations were considered.

First, using the Cartesian code VORPAL with a newly developed perfect dispersion algorithm (Cowan *et al.* 2012), VORPAL-PD, made it possible to use large grid spacings (~ 15 grid points per wavelength in the direction of propagation) and proportionally larger time steps. This approach reproduces the correct group velocity of a broad-bandwidth laser pulse. The red-shift, self-compression, and depletion of the laser pulse were thus described correctly, with proper resolution of all important physical scales.

Second, the well-preserved axial symmetry of the problem allowed us to use a re-

duced geometry description, with poloidal-mode decomposition of currents and fields. This approach was realised in the code CALDER-CIRC (Lifschitz *et al.* 2009). By using only two modes, we approached the performance of a 2D code, at the same time preserving the correct cylindrical geometry of the interaction. The high computational efficiency of CALDER-CIRC allowed us to use a very high longitudinal resolution (~ 50 grid points per laser wavelength in the direction of propagation) and a large number of macroparticles (~ 50 per cylindrical cell), eliminating numerical dispersion and strongly reducing the sampling noise. This high resolution simulation did not indicate any new physical effects relative to the VORPAL-PD runs, and did not exhibit significant differences in the quantitative results. Even with strong violation of cylindrical symmetry (such as near the dephasing limit, when the pulse was transformed into a two-cycle relativistic piston), the CALDER-CIRC results remained qualitatively correct.

Both codes described precisely the self-focusing of the laser pulse, the oscillations of its spot size, and related oscillations of the bubble; electron self-injection into the oscillating bubble and formation of a quasi-monoenergetic bunch; laser pulse frequency broadening and self-compression into the relativistic piston; constant elongation of the bubble during the piston formation; and uninterrupted electron injection eventually overloading the bubble. The codes showed excellent agreement on the locations of initiation and extinction of injection, on the collection volume, and on parameters of the quasi-monoenergetic component in the electron spectrum, indicating that the results are free of numerical artefacts. It is especially interesting that the CALDER-CIRC simulation with just two poloidal modes did not lose accuracy and preserved the correct group velocity (agreeing with the VORPAL-PD run) even when the laser pulse was compressed down two cycles.

We thus conclude that (1) using perfect dispersion, taking a coarser grid and larger time steps, and using higher-order splines for macroparticle shapes to suppress the sampling noise, or (2) neglecting high-order non-axisymmetric field and current components, thus reducing the dimensionality of problem are both effective and promising means to increase the computational efficiency without sacrificing fidelity. Both of these methods are applicable to the design of upcoming experiments on GeV-scale acceleration of electrons with 100 TW-scale lasers.

The work of B. M. C. and D. L. B. was partially supported by U. S. DOE Contract No. de-sc0006245 (SBIR). The work of S. Y. K. and B. A. S. was partially supported by U. S. DOE Contract No. DE-FG02-08ER55000 and by NSF Grant PHY-1104683. X. D. and A. F. L. thank Victor Malka for his support during the development of CALDER-CIRC. A. B. and E. L. acknowledge the support of LASERLAB-EUROPE/LAPTECH through EC FP7 contract no. 228334. The CALDER-CIRC simulations in this work were performed using high-performance computing resources of GENCI-CCRT (grant 2010-x2010056304). VORPAL simulations used resources of the National Energy Research Scientific Computing Center, which is supported by the Office of Science of the U. S. DOE under Contract No. DE-AC02-05CH11231.

REFERENCES

- ANDREEV, N. E., GORBUNOV, L. M., MORA, P. & RAMAZASHVILI, R. R. 2007 Filamentation of ultrashort laser pulses propagating in tenuous plasmas. *Phys. Plasmas* **14**, 083104.
- BIRDSALL, C. K. & LANGDON, A. B. 1985 *Plasma Physics via Computer Simulation*. New York, NY: McGraw-Hill.
- CIPICCIA, S., ISLAM, M. R., ERSFELD, B., SHANKS, R. P., BRUNETT, E., VIEUX, G., YANG, X., ISSAC, R. C., WIGGINS, S. M., WELSH, G. H., ANANIA, M.-P., MANEUSKI, D., MONTGOMERY, R., SMITH, G., HOEK, M., HAMILTON, D. J., LEMOS, N. R. C., SYMES,

- D., RAJEEV, P. P., SHEA, V. O., DIAS, J. M. & JAROSZYNSKI, D. A. 2011 Gamma-rays from harmonically resonant betatron oscillations in a plasma wake. *Nat. Phys.* **7**, 867–871.
- CLAYTON, C. E., RALPH, J. E., ALBERT, F., FONSECA, R. A., GLENZER, S. H., JOSHI, C., LU, W., MARSH, K. A., MARTINS, S. F., MORI, W. B., PAK, A., TSUNG, F. S., POLLOCK, B. B., ROSS, J. S., SILVA, L. O. & FROULA, D. H. 2010 Self-guided laser wakefield acceleration beyond 1 GeV using ionization-induced injection. *Phys. Rev. Lett.* **105**, 105003.
- CORMIER-MICHEL, E., SHADWICK, B. A., GEDDES, C. G. R., ESAREY, E., SCHROEDER, C. B. & LEEMANS, W. P. 2008 Unphysical kinetic effects in particle-in-cell modeling of laser wakefield accelerators. *Phys. Rev. E* **78** (1), 016404.
- COURANT, R., FRIEDRICHS, K. & LEWY, H. 1967 On the partial difference equations of mathematical physics. *IBM J. Res. Develop.* **11**, 215–234.
- COWAN, B. M. *et al.* 2012 Generalized algorithm for control of numerical dispersion in explicit time-domain electromagnetic simulations. *in preparation*.
- CUMMINGS, P. & THOMAS, A. G. R. 2011 A computational investigation of the impact of aberrated Gaussian laser pulses on electron beam properties in laser-wakefield acceleration experiments. *Phys. Plasmas* **18**, 053110.
- ESAREY, E., SCHROEDER, C. B. & LEEMANS, W. P. 2009 Physics of laser-driven plasma-based electron accelerators. *Rev. Mod. Phys.* **81** (3), 1229–1285.
- FAURE, J., GLINEC, Y., PUKHOV, A., KISELEV, S., GORDIENKO, S., LEFEBVRE, E., ROUSSEAU, J.-P., BURG, F. & MALKA, V. 2004 A laser-plasma accelerator producing monoenergetic electron beams. *Nature* **431**, 541.
- FAURE, J., GLINEC, Y., SANTOS, J. J., EWALD, F., ROUSSEAU, J.-P., KISELEV, S., PUKHOV, A., HOSOKAI, T. & MALKA, V. 2005 Observation of laser-pulse shortening in nonlinear plasma waves. *Phys. Rev. Lett.* **95**, 205003.
- FOURMAUX, S., CORDE, S., PHUOC, K. TA, LASSONDE, P., LEBRUN, G., PAYEUR, S., MARTIN, F., SEBBAN, S., MALKA, V., ROUSSEAU, A. & KIEFFER, J. C. 2011 Single shot phase contrast imaging using laser-produced betatron x-ray beams. *Opt. Lett.* **36**, 2426–2428.
- FROULA, D. H., CLAYTON, C. E., DÖPPNER, T., MARSH, K. A., BARTY, C. P. J., DIVOL, L., FONSECA, R. A., GLENZER, S. H., JOSHI, C., LU, W., MARTINS, S. F., MICHEL, P., MORI, W. B., PALASTRO, J. P., POLLOCK, B. B., PAK, A., RALPH, J. E., ROSS, J. S., SIDERS, C. W., SILVA, L. O. & WANG, T. 2009 Measurements of the critical power for self-injection of electrons in a laser wakefield accelerator. *Phys. Rev. Lett.* **103**, 215006.
- FUCHS, M., WEINGARTNER, R., POPP, A., MAJOR, ZS., BECKER, S., OSTERHOFF, J., CORTRIE, I., ZEITLER, B., HÖRLEIN, R., TSAKIRIS, G. D., SCHRAMM, U., ROWLANDS-REES, T. P., HOOKER, S. M., HABS, D., KRAUSZ, F., KARSCH, S. & GRÜNER, F. 2009 Laser-driven soft-X-ray undulator source. *Nat. Phys.* **5**, 826–829.
- GEDDES, C. G. R., TOTH, CS., VAN TILBORG, J., ESAREY, E., SCHROEDER, C. B., BRUH-WILER, D. L., NIETER, C., CARY, J. R. & LEEMANS, W.P. 2004 High-quality electron beams from a laser wakefield accelerator using plasma-channel guiding. *Nature* **431**, 538.
- GLINEC, Y., FAURE, J., LIFSCHITZ, A., VIEIRA, J. M., FONSECA, R. A., SILVA, L. O. & MALKA, V. 2008 Direct observation of betatron oscillations in a laser-plasma electron accelerator. *Europhys. Lett.* **81**, 64001.
- GORBUNOV, L. M., KALMYKOV, S. YU. & MORA, P. 2005 Laser wakefield acceleration by petawatt ultrashort laser pulses. *Phys. Plasmas* **12**, 033101.
- GORBUNOV, L. M. & KIRSANOV, V. I. 1987 Excitation of plasma waves by an electromagnetic wave packet. *Sov. Phys. JETP* **66**, 290–294.
- GORDIENKO, S. & PUKHOV, A. 2005 Scalings for ultrarelativistic laser plasmas and quasimonoenergetic electrons. *Phys. Plasmas* **12** (4), 043109.
- GRÜNER, F., BECKER, S., SCHRAMM, U., EICHNER, T., FUCHS, M., WEINGARTNER, R., HABS, D., MEYER-TER-VEHN, J., GEISSLER, M., FERRARIO, M., SERAFINI, L., VAN DER GEER, B., BACKE, H., LAUTH, W. & REICHE, S. 2007 Design considerations for table-top, laser-based VUV and X-ray free electron lasers. *Appl. Phys. B* **86** (3), 431–435.
- HAFZ, N. A. M., JEONG, T. M., CHOI, I. W., LEE, S. K., PAE, K. H., KULAGIN, V. V., SUNG, J. H., YU, T. J., HONG, K.-H., HOSOKAI, T., CARY, J. R., KO, D.-K. & LEE, J. 2008 Stable generation of GeV-class electron beams from self-guided laser-plasma channels. *Nat. Photonics* **2** (9), 571–577.

- HAFZ, N. A. M., LEE, S. K., JEONG, T. M. & LEE, J. 2011 Evolution of self-injected quasi-monoenergetic electron beams in a plasma bubble. *Nucl. Instrum. Methods A* **637**, S51–S53.
- HARTEMANN, F. V., GIBSON, D. J., BROWN, W. J., ROUSSE, A., TA PHUOC, K., MALKA, V., FAURE, J. & PUKHOV, A. 2007 Compton scattering x-ray sources driven by laser wakefield acceleration. *Phys. Rev. ST Accel. Beams* **10** (1), 011301.
- HIDDING, B., KÖNIGSTEIN, T., WILL, O., ROSENZWEIG, J. B., NAKAJIMA, K. & PRETZLER, G. 2011 Laser-plasma-accelerators—A novel, versatile tool for space radiation studies. *Nucl. Instrum. Methods A* **636**, 31–40.
- HOCKNEY, R. W. & EASTWOOD, J. W. 1981 *Computer Simulation Using Particles*. New York, NY: McGraw-Hill.
- KALMYKOV, S., YI, S. A., KHUDIK, V. & SHVETS, G. 2009 Electron self-injection and trapping into an evolving plasma bubble. *Phys. Rev. Lett.* **103** (13), 135004.
- KALMYKOV, S. Y., BECK, A., YI, S. A., KHUDIK, V. N., DOWNER, M. C., LEFEBVRE, E., SHADWICK, B. A. & UMSTADTER, D. P. 2011a Electron self-injection into an evolving plasma bubble: Quasi-monoenergetic laser-plasma acceleration in the blowout regime. *Phys. Plasmas* **18** (5), 056704.
- KALMYKOV, S. Y., SHADWICK, B. A., BECK, A. & LEFEBVRE, E. 2011b Physics of quasi-monoenergetic laser-plasma acceleration of electrons in the blowout regime. In *Femtosecond-Scale Optics* (ed. A. V. Andreev), pp. 113–138. InTech.
- KALMYKOV, S. Y., YI, S. A., BECK, A., LIFSCHITZ, A. F., DAVOINE, X., LEFEBVRE, E., KHUDIK, V., SHVETS, G. & DOWNER, M. C. 2011c Dark-current-free petawatt laser-driven wakefield accelerator based on electron self-injection into an expanding plasma bubble. *Plasma Phys. Control. Fusion* **53**, 014006.
- KALMYKOV, S. Y., YI, S. A., BECK, A., LIFSCHITZ, A. F., DAVOINE, X., LEFEBVRE, E., PUKHOV, A., KHUDIK, V., SHVETS, G., REED, S. A., DONG, P., WANG, X., DU, D., BEDACHT, S., ZGADZAJ, R., HENDERSON, W., BERNSTEIN, A., DYER, G., MARTINEZ, M., GAUL, E., DITMIRE, T. & DOWNER, M. C. 2010 Numerical modelling of a 10-cm-long multi-GeV laser wakefield accelerator driven by a self-guided petawatt pulse. *New J. Phys.* **12** (4), 045019.
- KÄRKKÄINEN, M., GJONAJ, E., LAU, T. & WEILAND, T. 2006 Low-dispersion wake field calculation tools. In *Proceedings of the 2006 International Computational Accelerator Physics Conference, Chamonix, France, 2006*, pp. 35–40.
- KARSCH, S., OSTERHOFF, J., POPP, A., ROWLANDS-REES, T P, MAJOR, Zs, FUCHS, M, MARX, B, HÖRLEIN, R, SCHMID, K, VEISZ, L, BECKER, S, SCHRAMM, U, HIDDING, B, PRETZLER, G, HABS, D, GRÜNER, F, KRAUSZ, F & HOOKER, S M 2007 GeV-scale electron acceleration in a gas-filled capillary discharge waveguide. *New J. Phys.* **9** (11), 415.
- KNEIP, S., MCGUFFEY, C., DOLLAR, F., BLOOM, M. S., CHVYKOV, V., KALINTCHENKO, G., KRUSHELNICK, K., MAKSIMCHUK, A., MANGLES, S. P. D., MATSUOKA, T., NAJMUDIN, Z., PALMER, C. A. J., SCHREIBER, J., SCHUMAKER, W., THOMAS, A. G. R., & YANOVSKY, V. 2011 X-ray phase contrast imaging of biological specimens with femtosecond pulses of betatron radiation from a compact laser plasma wakefield accelerator. *Appl. Phys. Lett.* **99**, 093701.
- KNEIP, S., MCGUFFEY, C., MARTINS, J. L., F, S. F., BELLEI, C., CHVYKOV, V., DOLLAR, F., FONSECA, R., HUNTINGTON, C., KALINTCHENKO, G., MAKSIMCHUK, A., MANGLES, S. P. D., MATSUOKA, T., NAGEL, S. R., PALMER, C. A. J., SCHREIBER, J., TA PHUOC, K., THOMAS, A. G. R., YANOVSKY, V., SILVA, L. O., KRUSHELNICK, K. & NAJMUDIN, Z. 2010 Bright spatially coherent synchrotron x-rays from a table-top source. *Nat. Phys.* **6**, 980–983.
- KNEIP, S., NAGEL, S. R., MARTINS, S. F., MANGLES, S. P. D., BELLEI, C., CHEKHLOV, O., CLARKE, R. J., DELERUE, N., DIVALL, E. J., DOUCAS, G., ERTEL, K., FIÚZA, F., FONSECA, R., FOSTER, P., HAWKES, S. J., HOOKER, C. J., KRUSHELNICK, K., MORI, W. B., PALMER, C. A. J., TA PHUOC, K., RAJEEV, P. P., SCHREIBER, J., STREETER, M. J. V., URNER, D., VIEIRA, J., SILVA, L. O. & NAJMUDIN, Z. 2009 Near-GeV acceleration of electrons by a nonlinear plasma wave driven by a self-guided laser pulse. *Phys. Rev. Lett.* **103**, 035002.
- LEEMANS, W. P., ESAREY, E., VAN TILBORG, J., MICHEL, P. A., SCHROEDER, C. B., TOTH, C., GEDDES, C. G. R. & SHADWICK, B. A. 2005 Radiation from laser accelerated electron

- bunches: coherent terahertz and femtosecond x-rays. *IEEE Trans. Plasma Science* **33** (1), 8–22.
- LEEMANS, W. P., NAGLER, B., GONSALVES, A. J., TOTH, Cs., NAKAMURA, K., GEDDES, C. G. R., ESAREY, E., SCHROEDER, C. B. & HOOKER, S. M. 2006 GeV electron beams from a centimetre-scale accelerator. *Nat. Phys.* **2** (10), 696–699.
- LEEMANS, W. P., RODGERS, D., CATRAVAS, P. E., GEDDES, C. G. R., FUBIANI, G., ESAREY, E., SHADWICK, B. A., DONAHUE, R. & SMITH, A. 2001 Gamma-neutron activation experiments using laser wakefield accelerators. *Phys. Plasmas* **8**, 2510–2516.
- LIFSCHITZ, A. F., DAVOINE, X., LEFEBVRE, E., FAURE, J., RECHATIN, C. & MALKA, V. 2009 Particle-in-cell modelling of laser-plasma interaction using Fourier decomposition. *J. Comput. Phys.* **228** (5), 1803–1814.
- LIU, J. S., XIA, C. Q., WANG, W. T., LU, H. Y., WANG, CH., DENG, A. H., LI, W. T., ZHANG, H., LIANG, X. Y., LENG, Y. X., LU, X. M., WANG, C., WANG, J. Z., NAKAJIMA, K., LI, R. X. & XU, Z. Z. 2011 All-optical cascaded laser wakefield accelerator using ionization-induced injection. *Phys. Rev. Lett.* **107**, 035001.
- LONTANO, M. & MURUSIDZE, I. G. 2003 Dynamics of space-time self-focusing of a femtosecond relativistic laser pulse in an underdense plasma. *Opt. Express* **11**, 248–258.
- LU, H., LIU, M., WANG, W., WANG, C., LIU, J., DENG, A., XU, J., XIA, C., LI, W., ZHANG, H., LU, X., WANG, C., WANG, J., LIANG, X., LENG, Y., SHEN, B., NAKAJIMA, K., LI, R. & XU, Z. 2011 Laser wakefield acceleration of electron beams beyond 1 GeV from an ablative capillary discharge waveguide. *Appl. Phys. Lett.* **99**, 091502.
- LU, W., HUANG, C., ZHOU, M., TZOUFRAS, M., TSUNG, F. S., MORI, W. B. & KATSOULEAS, T. 2006 A nonlinear theory for multidimensional relativistic plasma wave wakefields. *Phys. Plasmas* **13**, 056709.
- LU, W., TZOUFRAS, M., JOSHI, C., TSUNG, F. S., MORI, W. B., VIEIRA, J., FONSECA, R. A. & SILVA, L. O. 2007 Generating multi-GeV electron bunches using single stage laser wakefield acceleration in a 3D nonlinear regime. *Phys. Rev. ST Accel. Beams* **10** (6), 061301.
- MAKSIMCHUK, A., REED, S., BULANOV, S. S., CHVYKOV, V., KALINTCHENKO, G., MATSUOKA, T., MCGUFFEY, C., MOUROU, G., NAUMOVA, N., NEES, J., ROUSSEAU, P., YANOVSKY, V., KRUSHELNICK, K., MATLIS, N. H., KALMYKOV, S., SHVETS, G., DOWNER, M. C., VANE, C. R., BEENE, J. R., STRACENER, D., & SCHULTZ, D. R. 2008 Studies of laser wakefield structures and electron acceleration in underdense plasmas. *Phys. Plasmas* **15**, 056703.
- MANGLES, S. P. D., GENOUD, G., KNEIP, S., BURZA, M., CASSOU, K., CROS, B., DOVER, N. P., KAMPERIDIS, C., NAJMUDIN, Z., PERSSON, A., SCHREIBER, J., WOJDA, F. & WAHLSTRÖM, C.-G. 2009 Controlling the spectrum of x-rays generated in a laser-plasma accelerator by tailoring the laser wavefront. *Appl. Phys. Lett.* **95**, 181106.
- MANGLES, S. P. D., MURPHY, C. D., NAJMUDIN, Z., THOMAS, A. G. R., COLLIER, J. L., DANGOR, A. E., DIVALL, E. J., FOSTER, P. S., GALLACHER, J. G., HOOKER, C. J., JAROSZYNSKI, D. A., LANGLEY, A. J., MORI, W. B., NORREYS, P. A., TSUNG, F. S., VISKUP, R., WALTON, B. R. & KRUSHELNICK, K. 2004 Monoenergetic beams of relativistic electrons from intense laser-plasma interactions. *Nature* **431**, 535.
- MANGLES, S. P. D., THOMAS, A. G. R., LUNDH, O., LINDAU, F., KALUZA, M. C., PERSSON, A., WAHLSTRÖM, C.-G., KRUSHELNICK, K. & NAJMUDIN, Z. 2007 On the stability of laser wakefield electron accelerators in the monoenergetic regime. *Phys. Plasmas* **14** (5), 056702.
- MARTINS, S. F., FONSECA, R. A., LU, W., MORI, W. B. & SILVA, L. O. 2010 Exploring laser-wakefield-accelerator regimes for near-term lasers using particle-in-cell simulation in Lorentz-boosted frames. *Nat. Phys.* **6**, 311.
- MORA, P. & ANTONSEN, JR., THOMAS M. 1996 Electron cavitation and acceleration in the wake of an ultraintense, self-focused laser pulse. *Phys. Rev. E* **53**, R2068–R2071.
- NERUSH, E. N. & KOSTYUKOV, I. YU. 2009 Carrier-envelope phase effects in plasma-based electron acceleration with few-cycle laser pulses. *Phys. Rev. Lett.* **103**, 035001.
- NIETER, C. & CARY, J. R. 2004 VORPAL: A versatile plasma simulation code. *J. Comput. Phys.* **196**, 538.
- OGUCHI, A., ZHIDKOV, A., TAKANO, K., HOTTA, E., NEMOTO, K. & NAKAJIMA, K. 2008 Multiple self-injection in the acceleration of monoenergetic electrons by a laser wake field. *Phys. Plasmas* **15**, 043102.
- PAI, C.-H., CHANG, Y.-Y., HA, L.-C., XIE, Z.-H., LIN, M.-W., LIN, J.-M., CHEN, Y.-M.,

- TSAUR, G., CHU, H.-H., CHEN, S.-H., LIN, J.-Y., WANG, J. & CHEN, S.-Y. 2010 Generation of intense ultrashort midinfrared pulses by laser-plasma interaction in the bubble regime. *Phys. Rev. A* **82**, 063804.
- POLLOCK, B. B., CLAYTON, C. E., RALPH, J. E., ALBERT, F., DAVIDSON, A., DIVOL, L., FILIP, C., GLENZER, S. H., HERPOLDT, K., LU, W., MARSH, K. A., MEINECKE, J., MORI, W. B., PAK, A., RENSINK, T. C., ROSS, J. S., SHAW, J., TYNAN, G. R., JOSHI, C., & FROULA, D. H. 2011 Demonstration of a narrow energy spread, ~ 0.5 GeV electron beam from a two-stage laser wakefield accelerator. *Phys. Rev. Lett.* **107**, 045001.
- POPP, A., VIEIRA, J., OSTERHOFF, J., MAJOR, ZS., HÖRLEIN, R., FUCHS, M., WEINGARTNER, R., ROWLANDS-REES, T. P., MARTI, M., FONSECA, R. A., MARTINS, S. F., SILVA, L. O., HOOKER, S. M., KRAUSZ, F., GRÜNER, F., & KARSCH, S. 2010 All-optical steering of laser-wakefield-accelerated electron beams. *Phys. Rev. Lett.* **105**, 215001.
- PUKHOV, A., AN DER BRÜGGE, D. & KOSTYUKOV, I. 2010 Relativistic laser plasmas for electron acceleration and short wavelength radiation generation. *Plasma Phys. Control. Fusion* **52**, 124039.
- PUKHOV, A. & MEYER-TER-VEHN, J. 2002 Laser wake field acceleration: the highly non-linear broken-wave regime. *Appl. Phys. B* **74**, 355–361.
- PUKHOV, A. J. 1999 Three-dimensional electromagnetic relativistic particle-in-cell code VLPL (Virtual Laser Plasma Lab). *J. Plasma Phys.* **61** (03), 425–433.
- RAMANATHAN, V., BANERJEE, S., POWERS, N., CUNNINGHAM, N., CHANDLER-SMITH, N. A., ZHAO, K., BROWN, K., UMSTADTER, D., CLARKE, S., POZZI, S., BEENE, J., VANE, C. R. & SCHULTZ, D. 2010 Submillimeter-resolution radiography of shielded structures with laser-accelerated electron beams. *Phys. Rev. ST Accel. Beams* **13**, 104701.
- REED, S. A., CHVYKOV, V., KALINTCHENKO, G., MATSUOKA, T., YANOVSKY, V., VANE, C. R., BEENE, J. R., STRACENER, D., SCHULTZ, D. R. & MAKSIMCHUK, A. 2007 Efficient initiation of photonuclear reactions using quasimonoenergetic electron beams from laser wakefield acceleration. *J. Appl. Phys.* **102**, 073103.
- ROSENZWEIG, J. B., BREIZMAN, B., KATSOULEAS, T. & SU, J. J. 1991 Acceleration and focusing of electrons in two-dimensional nonlinear plasma wake fields. *Phys. Rev. A* **44**, R6189–R6192.
- ROUSSE, A., TA PHUOC, K., SHAH, R., FITOUR, R. & ALBERT, F. 2007 Scaling of betatron x-ray radiation. *Eur. Phys. J. D* **45**, 391–398.
- ROUSSE, A., TA PHUOC, K., SHAH, R., PUKHOV, A., LEFEBVRE, E., MALKA, V., KISELEV, S., BURG, F., ROUSSEAU, J.-P., UMSTADTER, D. & HULIN, D. 2004 Production of a keV X-ray beam from synchrotron radiation in relativistic laser-plasma interaction. *Phys. Rev. Lett.* **93** (13), 135005.
- SCHLENVOIGT, H.-P., HAUPT, K., DEBUS, A., BUDDE, F., JACKEL, O., PFOTENHAUER, S., GALLACHER, J.G., BRUNETTI, E., SHANKS, R.P., WIGGINS, S.M., JAROSZYNSKI, D.A., ROHWER, E. & SCHWOERER, H. 2008a Synchrotron radiation from laser-accelerated monoenergetic electrons. *IEEE Trans. Plasma Science* **36** (4), 1773–1781.
- SCHLENVOIGT, H.-P., HAUPT, K., DEBUS, A., BUDDE, F., JACKEL, O., PFOTENHAUER, S., SCHWOERER, H., ROHWER, E., GALLACHER, J. G., BRUNETTI, E., SHANKS, R. P., WIGGINS, S. M. & JAROSZYNSKI, D. A. 2008b A compact synchrotron radiation source driven by a laser-plasma wakefield accelerator. *Nat. Phys.* **4** (2), 130–133.
- SPRANGLE, P., ESAREY, E. & TING, A. 1990 Nonlinear interaction of intense laser pulses in plasmas. *Phys. Rev. A* **41** (8), 4463–4469.
- SUN, G.-Z., OTT, E., LEE, Y. C. & GUZDAR, P. 1987 Self-focusing of short intense pulses in plasmas. *Phys. Fluids* **30**, 526–532.
- TA PHUOC, K., BURG, F., ROUSSEAU, J.-P., MALKA, V., ROUSSE, A., SHAH, R., UMSTADTER, D., PUKHOV, A. & KISELEV, S. 2005 Laser based synchrotron radiation. *Phys. Plasmas* **12** (2), 023101.
- TAFLOVE, A. & HAGNESS, S. C. 2005 *Computational Electrodynamics: The Finite-Difference Time-Domain Method*, 3rd edn. Boston: Artech House.
- TAJIMA, T. & DAWSON, J. M. 1979 Laser electron accelerator. *Phys. Rev. Lett.* **43** (4), 267–270.
- THOMAS, A. G. R., MANGLES, S. P. D., MURPHY, C. D., DANGOR, A. E., FOSTER, P. S., GALLACHER, J. G., JAROSZYNSKI, D. A., KAMPERIDIS, C., KRUSHELNICK, K., LANCASTER, K. L., NORREYS, P. A., VISKUP, R. & NAJMUDIN, Z. 2009 Ultrashort pulse filamentation

- and monoenergetic electron beam production in LWFAs. *Plasma Phys. Control. Fusion* **51**, 024010.
- THOMAS, A. G. R., NAJMUDIN, Z., MANGLES, S. P. D., MURPHY, C. D., DANGOR, A. E., KAMPERIDIS, C., LANCASTER, K. L., MORI, W. B., NORREYS, P. A., ROZMUS, W. & KRUSHELNICK, K. 2007 Effect of laser-focusing conditions on propagation and monoenergetic electron production in laser-wakefield accelerators. *Phys. Rev. Lett.* **98** (9), 095004.
- TSUNG, F. S., LU, W., TZOUFRAS, M., MORI, W. B., JOSHI, C., VIEIRA, J. M., SILVA, L. O. & FONSECA, R. A. 2006 Simulation of monoenergetic electron generation via laser wakefield accelerators for 5–25 TW lasers. *Phys. Plasmas* **13** (5), 056708.
- TSUNG, F. S., REN, C., SILVA, L. O., MORI, W. B. & KATSOULEAS, T. 2002 Generation of ultra-intense single-cycle laser pulses by using photon deceleration. *Proc. Natl. Acad. Sci. U. S. A.* **99**, 29–32.
- VAY, J.-L., GEDDES, C. G. R., CORMIER-MICHEL, E. & GROTE, D. P. 2011 Numerical methods for instability mitigation in the modeling of laser wakefield accelerators in a Lorentz-boosted frame. *J. Comput. Phys.* **230** (15), 5908–5929.
- VIEIRA, J., FIÚZA, F., SILVA, L. O., TZOUFRAS, M. & MORI, W. B. 2010 Onset of self-steepening of intense laser pulses in plasmas. *New J. Phys.* **12**, 045025.
- WIGGINS, S. M., ISSAC, R. C., WELSH, G. H., BRUNETTI, E., SHANKS, R. P., ANANIA, M. P., CIPICCIA, S., MANAHAN, G. G., ANICULAESEI, C., ERSFELD, B., ISLAM, M. R., BURGESS, R. T. L., VIEUX, G., GILLESPIE, W. A., MACLEOD, A. M., VAN DER GEER, S. B., DE LOOS, M. J. & JAROSZYNSKI, D. A. 2010 High quality electron beams from a laser wakefield accelerator. *Plasma Phys. Control. Fusion* **52**, 124032.
- WU, H.-C., XIE, B.-S., LIU, M.-P., HONG, X.-R., ZHANG, S. & YU, M. Y. 2009 Electron trajectories and betatron oscillation in the wake bubble in laser-plasma interaction. *Phys. Plasmas* **16**, 073108.
- XU, H., YU, W., LU, P., SENECHA, V. K., HE, F., SHEN, B., QIAN, L., LI, R. & XU, Z. 2005 Electron self-injection and acceleration driven by a tightly focused intense laser beam in an underdense plasma. *Phys. Plasmas* **12**, 013105.
- YANOVSKY, V., CHVYKOV, V., KALINCHENKO, G., ROUSSEAU, P., PLANCHON, T., MATSUOKA, T., MAKSIMCHUK, A., NEES, J., CHERIAUX, G., MOUROU, G. & KRUSHELNICK, K. 2008 Ultra-high intensity 300-TW laser at 0.1 Hz repetition rate. *Opt. Express* **16**, 2109–2114.
- YEE, K. S. 1966 Numerical solution of initial boundary value problems involving Maxwell's equations in isotropic media. *IEEE Trans. Antennas Propag.* **14** (3), 302–307.
- ZAGORODNOV, I., SCHUHMAN, R. & WEILAND, T. 2003 Long-time numerical computation of electromagnetic fields in the vicinity of a relativistic source. *J. Comput. Phys.* **191**, 525–541.
- ZAGORODNOV, I. & WEILAND, T. 2005 TE/TM field solver for particle beam simulations without numerical Cherenkov radiation. *Phys. Rev. ST Accel. Beams* **8** (4), 042001.
- ZHIDKOV, A., KOGA, J., HOSOKAI, T., FUJII, T., OISHI, Y., NEMOTO, K. & KODAMA, R. 2010 Characterization of electron self-injection in laser wake field acceleration due to the parametric resonance. *Phys. Plasmas* **17**, 083101.